THE EUROPEAN
PHYSICAL JOURNAL PLUS

Check for
updates

Frequency-dependent damped vibrations of multifunctional foam plates sandwiched and integrated by composite faces

Babak Safaei[1,2,a]

[1] Department of Mechanical Engineering, Eastern Mediterranean University, Famagusta, North Cyprus via Mersin 10, Turkey
[2] Department of Mechanical Engineering Science, University of Johannesburg, Gauteng 2006, South Africa

Abstract This paper investigates damped vibrational behavior of a lightweight sandwich plate subjected to a periodic load within a limited time. The lightweight sandwich structure includes a thick polymeric porous core with either functionally graded or uniformly distributions of voids which is sandwiched by two thin layers of laminate composites. To investigate the effect of void distribution properly, the same void volume fraction has been considered while different types of core have been analyzed. Using the first-order shear deformation theory of plates, the governing equations for the free and forced vibrations have been developed. By involving structural damping, these equations which are able to treat thin to moderately thick plates have been solved by developing a computationally cost-effective finite element approach. An extensive sensitivity analysis has been performed to examine the effects of fiber orientation in composite layers, void's volume and dispersion in core, and geometrical dimensions on the vibrational behavior of such porous composite sandwich plates (PCSPs). The results show that the use of foam in PCSPs considerably reduces the amplitude of vibrations and improves the fundamental frequency. Furthermore, it was found that the use of $[45, -45]_2$ composite layers offers PCSPs with the highest natural frequency and the lowest amplitude of vibrations.

1 Introduction

Lightweight structures have been encountered with steadily growing demands over the last decades [1–3]. These growing demands are mainly observed in the aerospace industry which is one of the most promising industries [4, 5]. To address such demands, different types of materials include but not limited to fiber-reinforced composites, laminates, foams, and nanocomposite [6–10]. The performance of an engineering structure can be intensified by a suitable use of such materials [11]. Sandwich structures as promising engineering structures usually involve two thin but stiff outer layers to stand against normal loads, whereas a thick and usually soft material/structure is utilized as the core layer to ensure the stability of the structure against shear loads [12–14]. Due to the layer arrangements of sandwich panels,

[a] e-mail: babak.safaei@emu.edu.tr (corresponding author)

Springer

they enjoy a high ratio of structural stiffness to weight, and also their energy absorption is relatively high [15–17]. Given these facts about the sandwich structures, it can be anticipated that the use of composite and polymeric foam materials could be great selections to come up with a lightweight structure that is able to address so many requirements of an aerospace structure. The key design parameters for such sandwich structures could be fiber orientations of composite layers and geometrical dimensions. Moreover, in advanced foams, the distribution of voids can be controlled to follow FG patterns and adjust the mechanical or thermal performance of such structures [18–20]. However, the design of such functionally graded porous composite sandwich structures necessitates precise but simple mechanical analyses [21–24].

Because of the vast applications of composites, there have been so many works on the thermomechanical behaviors of composites structures. Mantari et al. [25] employed trigonometric theory and presented a Navier' solution for composite plates under static loads. In a dynamic study, Malekzadeh et al. [26] presented the response of a composite plate under moving loads by implementing a layerwise theory. Setoodeh [27] implemented three-dimensional theory of plates in a layerwise FE solution and studied low velocity impact response of composite plates. Thai et al. [28] investigated the stresses and static deflections of circular and rectangular composite plates using an isogeometric FE solution based on layerwise deformation theory which employed FSDT for each layer to avoid the use of shear correction factor. For composite plates with different shapes of holes, Yu et al. [29] presented buckling resistances and frequencies using an isogeometric FE solution and FSDT which was able to rectify the shear locking issue. Tornabene et al. [30] presented a differential quadrature (DQ) technique which captured the zig-zag effect between layers and presented stresses of curved shells consisted of different composite layers rested on elastic foundations. The static response [31] and free vibration behavior [32] of multilayered composite plates were also studied by Xiaohui et al. using a refined plate theory. Bisheh and Wu [33] studied the wave propagation behavior of composite shells which were activated by an outer piezoelectric layer using Cooper-Naghdi shell theory.

Polymeric foams or metal porous structures have been also widely utilized as the core layer of sandwich structures. However, before the use of these materials, their material properties need to be characterized. In this regard, Wang et al. [34] managed to simulate 3D voids in a media by developing an extended FEM modeling. Nguyen et al. [35] considered FG plates made of a mixture of metal and ceramic materials which had FG patterns of porosity distribution and characterized their mechanical behaviors using a nonlinear polygonal FE solution. Yang et al. [36] considered graphene enhanced plates with FG patterns of porosity distribution and presented vibration and buckling responses of such plates using an FSDT method. Dong et al. [37] proposed the use of the same material for rotary cylindrical shells and characterized vibrations of such porous nanocomposite shells. Barati and Zenkour [38] conducted a nonlinear free vibration analysis FG plates made of two piezoceramics with embedded porosities in FG patterns using a refined plate theory. Askari et al. [39] considered an FG porous metal circular plate located between two piezoceramic layers and presented the fundamental frequencies of such active plates Mindlin plate theory. Mohammadi et al. [40] also considered two piezoelectric layers attached to the faces of an FG porous metal cylinder and presented static electro-mechanical stresses of these active cylinders. Moradi et al. [41–43] considered FG patterns of porosity distributions in CNT enhanced plates which were activated by piezoceramic layers and presented vibrations, static and buckling responses using a mesh-free method. Nguyen et al. [44] also used piezoceramic to activate a graphene enhanced metal plate with embedded porosities in FG patterns, and conducted active control study for such plates using FE model. Zhao et al. [45] developed a semi-

analytical technique based on Fourier series to characterize the vibrations of axisymmetric shells with embedded porosities in FG patterns. Zargar et al. [46] conducted an analytical study to investigate heat transfer behavior of porous metal fins using an axisymmetric model. By employing 3D elasticity theory in a framework of an analytical solution, Babaei et al. [47] studied the frequencies and transient responses of disks and panels made of an FG porous metallic material. For FG porous silicon beams in nanoscale, Xie et al. [1] studied resonance phenomenon through a nonlinear analysis using surface elasticity theory.

Due to the structural benefits of foams and composite materials, researchers have been greatly convinced to apply them separately or jointly in sandwich structures. Sobhani and Yas [48] presented the fundamental frequencies of a sandwich shell which involved an FG metal/ceramic core and two fiber reinforced faces. They assumed FG patterns for the variation of fiber orientation in the plies of composite layers. Moradi et al. [49, 50] considered an FG polymeric porous plate sandwiched between two graphene enhanced layers, whereas whole these three layers activated by two more layers of a piezoceramic. They presented the fundamental frequencies and damped forced vibrations of such sandwich plates using a meshless technique. Setoodeh et al. [51] also considered curved sandwich shells with the same layer arrangement while they utilized CNT enhanced nanocomposite instead of graphene one, and presented the fundamental frequencies of such sandwich shells using DQ technique. Safaei et al. [52] presented dynamic behavior of FG porous plates sandwiched between CNT enhanced nanocomposite layers using a third-order theory. Amiri et al. [53] considered a flexible porous cylindrical micropanel sandwiched between two CNT enhanced nanocomposite faces, and presented buckling resistance as well as stresses of the resulting micro-sandwich panel. Li et al. [54] enhanced a rectangular FG porous metal plate with graphene nanosheets and presented the dynamic stability resistance of the resulting sandwich structure through a nonlinear analysis. In a dynamic analysis framework, the propagation of stress waves in FG porous cylinders sandwiched by graphene enhanced layers was analyzed using a mesh-free method in [55]. Safaei [56] studied the impact of adding a thick FG polymeric foam in the middle of composite plies on the fundamental frequencies of the resulting sandwich plate while it was rested on an elastic foundation.

This paper investigates the natural frequencies and damped forced vibrations of an advanced and lightweight sandwich plate under a periodic load within a limited time. This sandwich plate includes a thick FG/UD polymeric core which is sandwiched by two thin layers of laminate composites. The governing equations for the study of dynamic behavior of the proposed PCSPs are developed using FSDT, and then these equations were treated using an FE solution. Using the mentioned solution approach, an extensive sensitivity analysis has been performed to examine the effects of fiber orientation in composite layers, void's volume and dispersion in core, and geometrical dimensions on the vibrational behavior of PCSPs.

2 Modeling of PCSP

As illustrated in Fig. 1, a sandwich plate with outer layers made of fiber-reinforced composite and a core made of a polymeric foam with FG/UD distributions of porosities have been considered. In addition, this PCSP is subjected to a sinusoidal periodic load i.e., $f(t) = f_0 \sin(2\pi \omega_t t)$ with the load amplitude f_0 and load frequency ω_t in a limited time ($t < t_0$) as shown in Fig. 2. The composite layers are assumed to be two layers composed of $2p$ plies which are indicated as $[\alpha_1, \alpha_2,]_p$. The considered PCSPs have side length a, thickness h, core thickness h_c and composite thickness h_f.
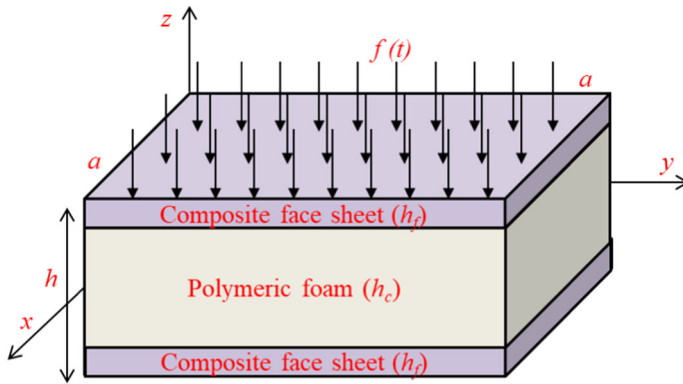
Fig. 1 The schematic of PLCSP with an FG foam sandwiched by two composite layers under a uniform load
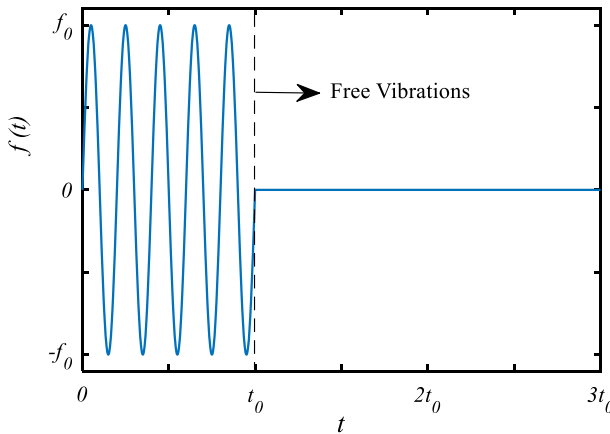
Fig. 2 Time history of the applied uniform load

2.1 Governing equations

By employing the first-order shear deformation theory which is capable of treating such sandwich plates when they are thin to moderately thick, the displacement field can be described only with five unknowns as follows ([57, 58]):

$$
\begin{aligned}
u &= u_0(x, y) + z\varphi_x(x, y) \\
v &= v_0(x, y) + z\varphi_y(x, y) \\
w &= w_0(x, y)
\end{aligned}
\tag{1}
$$

where u, v and w show components of the displacement field in Cartesian coordinates. Moreover, φ and the subscribe 0 show normal rotations and deflections of the midline of PCSP, respectively.

According to Eq. (1), the linear components of strain vector for the proposed PCSP are presented below [57]:

$$
\varepsilon_{xx} = \frac{\partial u}{\partial x}, \; \varepsilon_{yy} = \frac{\partial v}{\partial y}, \; \gamma_{xy} = \frac{\partial u}{\partial y} + \frac{\partial v}{\partial x}, \; \gamma_{xz} = \frac{\partial u}{\partial z} + \frac{\partial w}{\partial x}, \; \gamma_{yz} = \frac{\partial v}{\partial z} + \frac{\partial w}{\partial y}
\tag{2}
$$

To make the equations easier, the in-plane $\boldsymbol{\varepsilon}_b$ and out-of-plane $\boldsymbol{\gamma}$ components of the strain vector can be distinguished as follow:

$$\varepsilon_b = \left\{ \begin{array}{c} \partial u_0/\partial x \\ \partial v_0/\partial y \\ \partial u_0/\partial y + \partial v_0/\partial x \end{array} \right\} + z \left\{ \begin{array}{c} \partial \varphi_x/\partial x \\ \partial \varphi_y/\partial y \\ \partial \varphi_x/\partial y + \partial \varphi_y/\partial x \end{array} \right\} \quad \gamma = \left\{ \begin{array}{c} \varphi_x + \partial w_0/\partial x \\ \varphi_y + \partial w_0/\partial y \end{array} \right\} \quad (3)$$

or in the vector form, they are rewritten as:

$$\boldsymbol{\varepsilon}_b = \left\{ \varepsilon_{xx} \; \varepsilon_{yy} \; \gamma_{xy} \right\}^T = \boldsymbol{\varepsilon_0} + z\boldsymbol{\varepsilon_1} \;, \; \boldsymbol{\gamma} = \left\{ \gamma_{xz} \; \gamma_{yz} \right\}^T \quad (4)$$

In the same manner, the in-plane $\boldsymbol{\sigma}$ and out-of-plane $\boldsymbol{\tau}$ stress vectors of PCSPs are also distinguished in the constitutive equation as follows [57]:

$$\boldsymbol{\sigma} = \mathbf{D_b}\boldsymbol{\varepsilon}_b \;, \; \boldsymbol{\tau} = \frac{5}{6}\mathbf{D_s}\boldsymbol{\gamma} \;, \; \mathbf{D} = \begin{bmatrix} \mathbf{D_b} & 0 \\ 0 & \mathbf{D_s} \end{bmatrix} \quad (5)$$

where 5/6 is for the shear correction factor as it is needed in FSDT, and $\mathbf{D}$ is the elastic constant matrix. $\mathbf{D}$ and stress vectors are defined below:

$$\left\{ \begin{array}{c} \sigma_x \\ \sigma_y \\ \sigma_{xy} \end{array} \right\} = \begin{bmatrix} D_{11} & D_{12} & D_{16} \\ D_{12} & D_{22} & D_{26} \\ D_{26} & D_{26} & D_{66} \end{bmatrix} \left\{ \begin{array}{c} \varepsilon_x \\ \varepsilon_y \\ \gamma_{xy} \end{array} \right\} \left\{ \begin{array}{c} \tau_{xz} \\ \tau_{yz} \end{array} \right\} = \frac{5}{6} \begin{bmatrix} D_{55} & D_{45} \\ D_{45} & D_{44} \end{bmatrix} \left\{ \begin{array}{c} \gamma_{xz} \\ \gamma_{yz} \end{array} \right\} \quad (6)$$

Given the aforementioned equations for the displacement field, strains and stresses, the energy function U of the proposed PCSP which includes the energy of external work, kinetic energy and strain energy are defined as follows:

$$\Pi = \frac{1}{2} \int_{\Omega} \left[-\rho(z)(\dot{u}^2 + \dot{v}^2 + \dot{w}^2) + \boldsymbol{\varepsilon}_b^T \boldsymbol{\sigma} + \boldsymbol{\gamma}^T \boldsymbol{\tau} \right] d\Omega + \int_A w\mathbf{f}\, dA \quad (7)$$

where ρ is density, A is the area of PCSP that load is applied on it, and V is the volume of PCSP and is $\mathbf{f}$ the load vector.

2.2 Materials properties of foam layer

In order to define the components of $\mathbf{D}$ described in Eqs. (5) and (6), the material properties of each layer need to be defined. As mentioned before, one uniform pattern and two FG patterns including a symmetric (FG-S) and an asymmetric (FG-A) one for the distributions of porosity inside the foam layer have been considered. For further illustration, Fig. 3 generally compares such patterns along the thickness of the foam layer. According to Ref. [45], the density ρ^p and elasticity modulus E^p of such foams with these three distribution patterns can be estimated as:
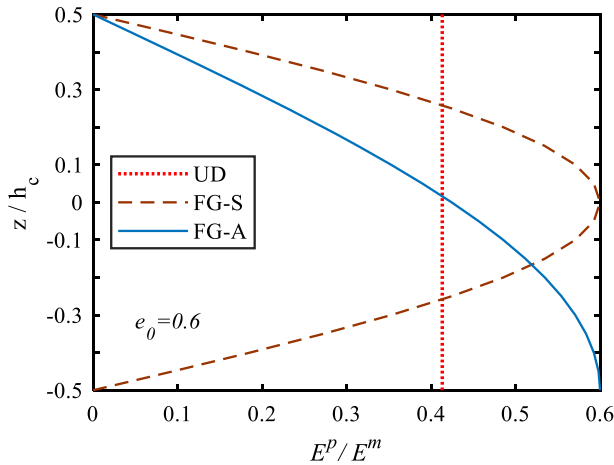
$$UD: E^P = \left(\frac{2}{\pi}\sqrt{1 - e_0} - \frac{2}{\pi} + 1 \right)^2 E^m \; \rho^P = \left(\frac{2}{\pi}\sqrt{1 - e_0} - \frac{2}{\pi} + 1 \right)\rho^m \quad (8)$$

$$FG - S: E^P(z) = \left(1 - e_0 \cos\left(\frac{\pi z}{h_c}\right) \right)E^m \; \rho^P(z) = \left(1 - e_m \cos\left(\frac{\pi z}{h_c}\right) \right)\rho^m \quad (9)$$

$$FG - A: E^P(z) = \left(1 - e_0 \cos\left(\frac{\pi z}{4h_c} + \frac{\pi}{4}\right) \right)E^m \; \rho^P(z) = \left(1 - e_m \cos\left(\frac{\pi z}{4h_c} + \frac{\pi}{4}\right) \right)\rho^m \quad (10)$$

in which Poisson's ratio of such foams υ^p is estimated as:

$$\upsilon^P(z) = 0.221\beta + \upsilon^m\left(0.342\beta^2 - 1.21\beta + 1\right) \quad (11)$$

Fig. 3 Comparison between the three porosity patterns with $e_0 = 0.6$

where e_0 and superscript m indicate porosity parameter a non-porous material (i.e., $e_0 = 0$). Moreover, $e_m = 1 - \sqrt{1 - e_0}$, $\beta = 1 - \rho^p/\rho^m$. It should be noted that the overall volume fraction of porosity for these three patterns is equal when the same e_0 is considered.

Given the fact that the foam layer is an isotropic material, the components of elasticity matrix D_{ij} are determined as follows:

$$D_{11} = D_{22} = \frac{E^p}{1 - (v^p)^2} \, , D_{44} = D_{55} = D_{66} = \frac{E^p}{2(1 + v^p)} \, ,$$

$$D_{12} = v^p D_{11} \, , D_{16} = D_{26} = D_{45} = 0 \tag{12}$$

2.3 Elasticity matrix of composite layers

The fiber-reinforced composite materials are usually a transverse isotropic material. Therefore, the elasticity matrix for such materials when the components of z direction are reduced can be defined as:

$$D_{ij} = \begin{cases} \overline{Q}_{ij} - (\overline{Q}_{i3} \cdot \overline{Q}_{ij})/Q_{33} & i, j = 1, 2, 6 \\ \overline{Q}_{ij} & i, j = 4, 5 \end{cases} \tag{13}$$

where

$$Q_{11} = E_1 \frac{1 - v_{23} v_{32}}{\Delta} \, , \quad Q_{22} = E_2 \frac{1 - v_{13} v_{31}}{\Delta} \, , \quad Q_{12} = E_1 \frac{v_{21} + v_{31} v_{32}}{\Delta} \, ,$$

$$Q_{13} = E_3 \frac{v_{13} + v_{12} v_{23}}{\Delta} \, , \quad Q_{23} = E_3 \frac{v_{23} + v_{13} v_{21}}{\Delta} \, , \quad Q_{33} = E_3 \frac{1 - v_{12} v_{21}}{\Delta}$$

$$Q_{44} = G_{23} \, , \quad Q_{55} = G_{13} \, , \quad Q_{66} = G_{12} \tag{14}$$

$$\Delta = \frac{1 - v_{32} v_{23} - v_{21} v_{12} - v_{13} v_{31} - 2 \, v_{32} v_{21} v_{13}}{E_1 E_2 E_3}$$

In order to take into account the effect of fiber orientation, another elasticity matrix $\overline{Q}_{ij}$ should be determined as follows [57]:

$$\overline{Q}_{11} = m^4 Q_{11} + 2m^2 n^2 (Q_{12} + 2Q_{66}) + n^4 Q_{22},$$

$$\overline{Q}_{22} = n^4 Q_{11} + 2m^2 n^2 (Q_{12} + 2 Q_{66}) + m^4 Q_{22}$$

$$\overline{Q}_{44} = m^2 Q_{44} + n^2 Q_{55}, \quad \overline{Q}_{55} = m^2 Q_{55} + n^2 Q_{44},$$

$$\overline{Q}_{66} = -m^2 n^2 (Q_{11} + Q_{22} - 2 Q_{12}) + (m^4 - n^4) Q_{66}$$

$$\overline{Q}_{12} = m^2 n^2 (Q_{11} + 4 Q_{22} Q_{66}) + (m^4 + n^4) Q_{12},$$

$$\overline{Q}_{13} = m^2 Q_{13} + n^2 Q_{23}, \quad \overline{Q}_{23} = n^2 Q_{13} + m^2 Q_{23}$$

$$\overline{Q}_{36} = (Q_{32} - Q_{31})mn, \quad \overline{Q}_{45} = (Q_{45} - Q_{55})mn,$$

$$\overline{Q}_{16} = -mn \left[n^2 Q_{11} - m^2 Q_{22} - (m^2 - n^2)(Q_{12} + 2 Q_{66}) \right]$$

$$\overline{Q}_{26} = -mn \left[m^2 Q_{11} - n^2 Q_{22} - (m^2 - n^2)(Q_{12} + 2 Q_{66}) \right] \tag{15}$$

where $m = \cos \alpha$ and $n = \sin \alpha$.

3 FEM Formulations

By employing a proper shape function **N**, the real values of displacement vector u_i can be estimated in an element as follows:

$$\mathbf{u} = \sum_{i=1}^{n} N_i u_i \tag{16}$$

where **u** is the estimated displacement field by FE method, N_i is value of shape functions at each node, n is node number in each element. Due to employing FSDT, each node has five degrees of freedom and accordingly the components of displacement field are defined as:

$$u_i = \left[u_{0i}, v_{0i}, w_{0i}, \varphi_{xi}, \varphi_{yi} \right]^T \tag{17}$$

By substituting Eq. (16) into Eq. (4), strain vectors in FE forms are developed as follows:

$$\boldsymbol{\varepsilon}_b = \{ \mathbf{P}_m + z \, \mathbf{P}_b \} \mathbf{u} \quad , \quad \boldsymbol{\gamma} = \mathbf{P}_s \, \mathbf{u} \tag{18}$$

where:

$$\mathbf{P}_s = \begin{bmatrix} 0 & 0 & N_{i,x} & N_i & 0 \\ 0 & 0 & N_{i,y} & 0 & N_i \end{bmatrix}, \mathbf{P}_m = \begin{bmatrix} N_{i,x} & 0 & 0 & 0 & 0 \\ 0 & N_{i,y} & 0 & 0 & 0 \\ N_{i,y} & N_{i,x} & 0 & 0 & 0 \end{bmatrix}$$

$$\mathbf{P}_b = \begin{bmatrix} 0 & 0 & 0 & N_{i,x} & 0 \\ 0 & 0 & 0 & 0 & N_{i,y} \\ 0 & 0 & 0 & N_{i,y} & N_{i,x} \end{bmatrix} \tag{19}$$

The FE form of energy function can be obtained by substituting strain and stress vectors into total energy function (Eq. 7) which results in:

$$U = \frac{1}{2} \int_{\Omega} \delta(\mathbf{u})^T \left\{ \mathbf{P}_m^T \mathbf{A} \mathbf{P}_m + \mathbf{P}_m^T \overline{\mathbf{B}} \mathbf{P}_b + \mathbf{P}_b^T \overline{\mathbf{B}} \mathbf{P}_m + \mathbf{P}_b^T \mathbf{D} \mathbf{B}_b + \mathbf{P}_s^T \mathbf{A}_s \mathbf{P}_s \right\} \mathbf{u} \, dA$$

$$+ \frac{1}{2} \int_{A} \delta(\mathbf{u})^T \int_{z} \left[\mathbf{I}_i^T \overline{\mathbf{M}} \mathbf{I}_j \right] \mathbf{R} \, dA - \delta(\mathbf{u})^T \int_{\Omega} \mathbf{P}_w \, \mathbf{f}_w \, dA \tag{20}$$

where

$$(\mathbf{A}, \overline{\mathbf{B}}, \mathbf{D}) = \int\limits_{-h/2}^{h/2} \mathbf{D}_b(1, z, z^2)dz \ , \ \mathbf{A}_s = \frac{5}{6} \int\limits_{-h/2}^{h/2} \mathbf{D}_s dz \tag{21}$$

$$\mathbf{P}_w = \begin{bmatrix} 0 & 0 & N_i & 0 & 0 \end{bmatrix} \tag{22}$$

$$\mathbf{I}_i = \begin{bmatrix} N_i & 0 & 0 & 0 & 0 \\ 0 & N_i & 0 & 0 & 0 \\ 0 & 0 & N_i & 0 & 0 \\ 0 & 0 & 0 & N_i & 0 \\ 0 & 0 & 0 & 0 & N_i \end{bmatrix} \tag{23}$$

$$\overline{\mathbf{M}} = \begin{bmatrix} I_0 & 0 & 0 & I_1 & 0 \\ 0 & I_0 & 0 & 0 & I_1 \\ 0 & 0 & I_0 & 0 & 0 \\ I_1 & 0 & 0 & I_2 & 0 \\ 0 & I_1 & 0 & 0 & I_2 \end{bmatrix} \tag{24}$$

In addition, I_0, I_1 and I_2 are the coefficient of inertia which are defined as:

$$(I_0, I_1, I_2) = \int\limits_{-h/2}^{h/2} \rho(z)(1, z, z^2)dz \tag{25}$$

Equation (20) should be satisfied for every value of $\delta(\mathbf{u})$; therefore this equation can be rearranged as:

$$\mathbf{M}\ddot{\mathbf{u}} + \mathbf{Ku} = \mathbf{f} \tag{26}$$

where $\mathbf{f}$, $\mathbf{M}$ and $\mathbf{K}$ are the global force vector, stiffness matrix and mass matrix as described below:

$$\mathbf{f} = \int\limits_{\Omega} \mathbf{P}_w \mathbf{f}_w \, dA \tag{27}$$

$$\mathbf{M} = \int\limits_{A} \mathbf{I}_i^T \overline{\mathbf{M}} \mathbf{I}_j dA \tag{28}$$

$$\mathbf{K} = \int\limits_{\Omega} \left\{ \mathbf{B}_m^T \mathbf{A} \mathbf{B}_m + \mathbf{B}_m^T \overline{\mathbf{B}} \mathbf{B}_b + \mathbf{B}_b^T \overline{\mathbf{B}} \mathbf{B}_m + \mathbf{B}_b^T \mathbf{D} \mathbf{B}_b + \mathbf{B}_s^T \mathbf{A}_s \mathbf{B}_s \right\} d\Omega \tag{29}$$

By involving structural damping with mass Rm and stiffness Rk coefficients, Eq. (26) is rearranged as follows:

$$\mathbf{M}\ddot{\mathbf{u}} + \mathbf{C}\dot{\mathbf{u}} + \mathbf{Ku} = \mathbf{f} \tag{30}$$

where $\mathbf{C} = Rm \times \mathbf{M} + Rk \times \mathbf{K}$.

4 Results and discussions

After the elaboration of the problem and its solution procedure in previous sections, the free and forced vibration behaviors of the proposed lightweight sandwich plates as well as the reliability of the developed FE approach are presented in this section. Regarding the

Table 1 comparison study for the normalized natural frequency of square isotropic plates

$h/a = 0.05$		$h/a = 0.1$		$h/a = 0.2$	
Method	Ω	Method	Ω	Method	Ω
[60]	0.0291	[60]	0.1134	[60]	0.4154
[61]	0.0291	[61]	0.1135	[61]	0.4154
Present study	0.0292	Present study	0.1136	Present study	0.4159

utilized materials in PCSP, a neat epoxy foam is considered for the core, whereas composite layers made of graphite–epoxy (Gr/Ep) is utilized for the face layers. The employed material properties for the nonporous epoxy and Gr/Ep are as follows [59]:

Epoxy : $E = 4.5$ GPa, $\upsilon = 0.4$, $\rho = 1150$ Kg/m^3

$Gr/Ep : E_{11} = 132.38$ GPa, $E_{12} = E_{13} = 10.756$ GPa, $\upsilon_{23} = 0.49$, $\upsilon_{12} = \upsilon_{13} = 0.24$,

$G_{23} = 3.606e9$ GPa, $G_{12} = G_{13} = 5.6537$ GPa, $\rho = 1578$ Kg/m^3

4.1 Validation of models

To establish the precision of the obtained FE results, we first modeled square simply supported plates made of an isotropic material with $E = 380$ GPa, $\rho = 3800$ kg/m^3 and $\upsilon = 0.3$ and compared the obtained normalized natural frequency of such plates at different thickness values with those available in Refs. [60, 61]. This comparison study has been summarized in Table 1, whereas the normalized natural frequency is determined by $\Omega = \omega h_0 \sqrt{\rho^m / E^m}$ where $h_0 = 0.1$ m. It is evident from the agreement between the results that the precision of the developed FE solution is successfully verified especially for thinner plates i.e., $h/a < 0.2$.

As a further establishment of the precision of the developed FE solution, we have examined the convergence of the results by studying time history of vibrations at the midpoint of a PCSP. Therefore, a simply supported (SSSS) square PCSP with $a = 1$ m, $h_c/a = 0.01$ and $h_f/h_c = 0.1$, whereas the PCSP has an FG-S core with $e_0 = 0.7$, and two composite faces with four plies as $[45,-45]_2$. Figure 4 shows the undamped vibrations of this PCSP under a periodic load with $f_0 = 500$ N/m^2, $t_0 = 100$ ms and $\omega_t = 50$ Hz for different node arrangements. This figure illustrates that the dynamic response of this plate is perfectly converged such that there is a slight difference between the results of models employed at higher nodes. Therefore, for the following modelings, PCSPs with 15×15 nodes have been considered.

4.2 Free vibration of PCSPs

This subsection concerns the study of the fundamental natural frequency of PCSPs. In the first analysis, the effect of fiber orientations is investigated. In this regard, SSSS square PCSPs with $a = 1$ m, $h_c/a = 0.01$, $h_f/h_c = 0.1$, $e_0 = 0.7$, FG-S porosity patterns and with composite faces with different fiber orientations and ply number have been considered. Table 2 summarizes the results of this study and shows that although the number of ply slightly improves the fundamental frequency, fiber orientation has a significant impact on it such that the fundamental frequency of PCSP with $[0,90]_2$ is only 67.02 Hz while this number for the same PCSP with $[45,-45]_2$ is 86.61 Hz. This shows fiber orientation can remarkably change the structural stiffness of PCSPs.
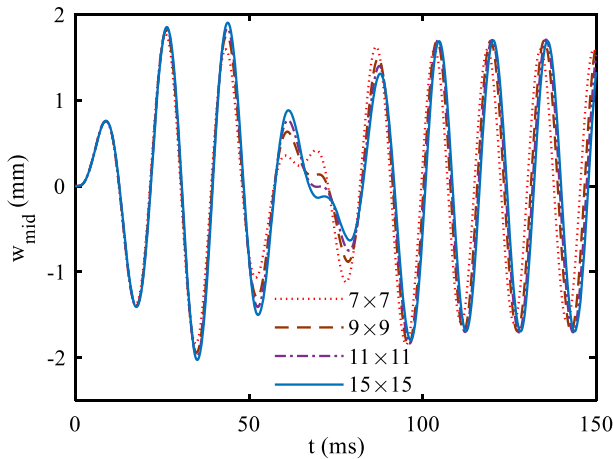
Fig. 4 midpoint undamped vibrations of a PCSP with different node arrangements (convergence study)

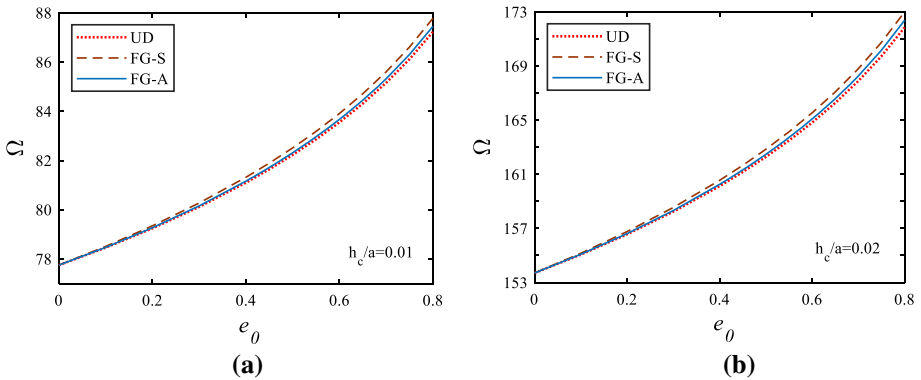| **Table 2** Fundamental frequencies (Hz) of PCSPs with different fiber orientations and ply numbers	p	1	2	3	4
	$[0, 90]p$	67.019	67.020	67.021	67.021
	$[15, -15]p$	71.954	72.031	72.045	72.050
	$[30, -30]p$	81.159	81.337	81.370	81.382
	$[45, -45]p$	85.390	85.607	85.647	85.661

Considering the same PCSPs but with $[45, -45]_2$ and different porosity parameters and distribution patterns, Figs. 5a and b study the effect of different porosity states for PCSPs with $h_c/a = 0.01$ and 0.02, respectively. The most important observation is that the increase in embedding porosity enhances the fundamental frequency of PCSPs due to the significant reduction of the weight of PCSPs. Moreover, the results show that PCSPs with FG-S foams in core offer the higher fundamental frequencies while those with UD foam have the lowest natural frequencies. Furthermore, as anticipated, the comparison between Figs. 5a and b discloses that the natural frequencies of PCSPs with thicker cores have greatly higher natural frequencies.
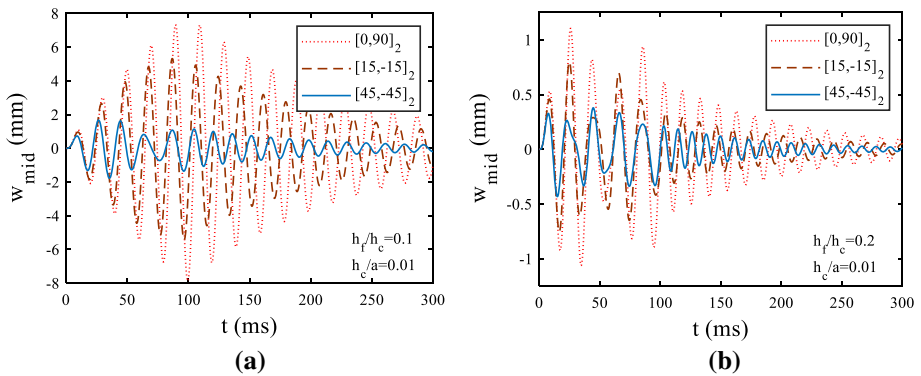
4.3 Forced vibrations of PCSPs

In this subsection, the forced vibration response of PCSPs is investigated. In the following modeling, SSSS square PCSP with geometrical dimensions as $a = 1$ m, $h_c/a = 0.01$ and $h_f/h_c = 0.1$, porosity states as FG-S core with $e_0 = 0.7$, composite faces with fiber orientation as [45,-45]$_2$, damping status as $Rm = 10$ and $Rk = 5e\text{-}5$, and loading conditions as $f_0 = 500$ N/m^2, $t_0 = 100$ ms and $\omega_t = 50$ Hz have been considered unless otherwise clearly mentioned.

To begin with, the effect of fiber orientation is investigated in Fig. 6 where the midpoint vibrations of PCSPs with different fiber orientations for two values of composite layers' thicknesses are shown. Figure 6 shows that PCSPs with [45,-45]$_2$ have the lowest vibration amplitudes while their frequencies of vibrations in the free vibration zone are the highest. On the other side, PCSPs with [0, 90]$_2$ can be observed whose vibrations have the highest

Fig. 5 Fundamental frequency of PCSPs with **a** $h_c/a = 0.01$ **b** $h_c/a = 0.02$ versus porosity parameter for different porosity distribution patterns
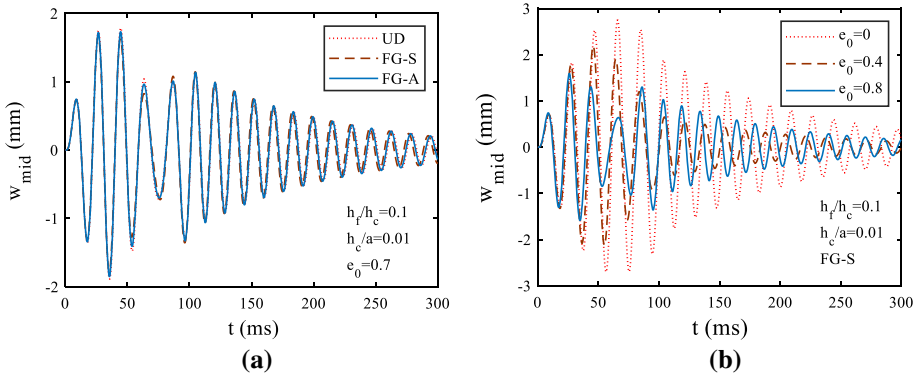

Fig. 6 Midpoint's vibrations of PCSPs with **a** $h_f/h_c = 0.1$ **b** $h_f/h_c = 0.2$ and different fiber orientations

amplitudes and the lowest frequencies of vibrations in the free vibration zone. These observations are absolutely supported by the results reported in Table 2. Moreover, the comparison between the vibrations of PCSPs with $h_f/h_c = 0.1$ and $h_f/h_c = 0.2$ reveals that the thickness of composite faces has a remarkable impact on both amplitudes and frequencies of vibrations.

Figures 7a and b also explore the effect of porosity distribution patterns and porosity parameters on the vibrations of the proposed PCSPs, respectively. Figure 7a shows that the pattern of porosity distribution does not have a considerable impact on the vibrations of PCSPs although PCSPs with UD core have vibrations with the highest amplitudes and the lowest frequency. On the other side, Fig. 7b illustrates that the amount of porosity embedded in the core layer has a great impact on the vibrations of PCSPs such that the PCSP with nonporous core has the lowest frequency of vibrations as this observation is supported with the results of Fig. 5. Moreover, it can be seen that PCSPs with porous cores have the lowest amplitudes of vibrations. This could be due the beats phenomena observed in forced vibration zone as the vibrations of PCSPs with porous core are entered into the free vibration zone with much lower amplitudes of vibrations.

Figure 8 also investigates the effect of structural damping coefficients on the vibrations of the PCSP. As expected, the application of each coefficient smoothly reduces the vibrations

Fig. 7 Midpoint's vibrations of PCSPs with different **a** porosity distribution patterns **b** porosity parameter
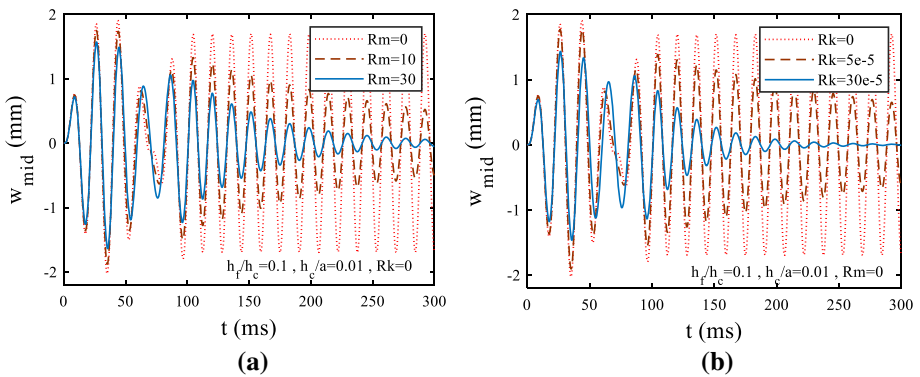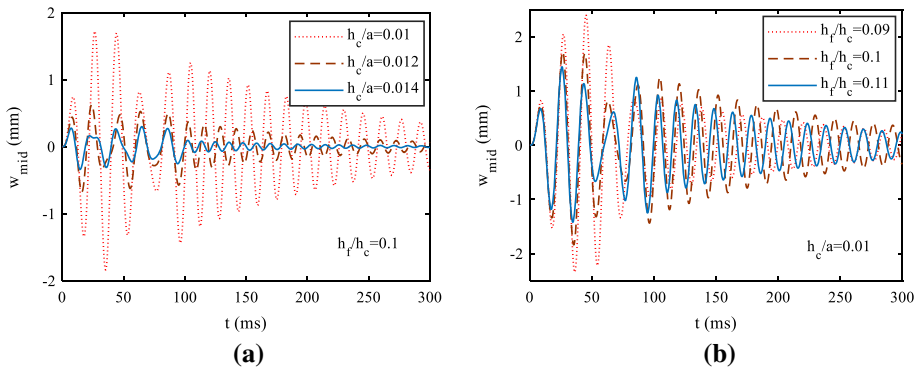

Fig. 8 Midpoint's vibrations of PCSPs with different **a** mass coefficient **b** stiffness coefficient of structural damping

amplitudes. It also observed that the frequency of vibrations is slightly reduced by increasing these coefficients. This figure also gives a good understanding about the range of structural damping coefficients.

Finally, the effects of core and face thicknesses on the vibrations are investigated in Figs. 9a and b, respectively. It can be seen the use of thicker layers either in core or faces leads to significant reductions in vibration amplitudes as well as a considerable increase in vibration frequencies as the structural stiffness of PCSPs improves.

5 Conclusions

Lightweight sandwich plates consist of two thin composite layer faces, and a thick polymeric foam core was considered. UD and FG patterns were considered for the distribution of porosities inside the thick foam layer. The natural frequency and damped forced vibration behavior of such advanced PCSPs under a periodic load within a limited time were investigated by developing an FE solution based on FSDT. By performing an extensive sensitivity analysis on the considered PCSP, it was found that simply supported PCSPs with the fiber orientation of $[45, -45]_2$ offer the highest natural frequency and the lowest amplitude of vibrations.

Fig. 9 Midpoint's vibrations of PCSPs with different **a** core thicknesses **b** composite layer thicknesses

Moreover, the results showed that the amount of porosity has a significant impact on both fundamental frequency and transient response of PCSPs such that embedding porosity reduces the amplitude of vibrations and improves the fundamental frequency. Furthermore, it was shown that the use of thicker layers leads to PCSPs with lower vibrations amplitudes and higher frequency of vibrations.

References

1. B. Xie, S. Sahmani, B. Safaei, B. Xu, Nonlinear secondary resonance of FG porous silicon nanobeams under periodic hard excitations based on surface elasticity theory. Eng. Comput. **37**, 1611–1634 (2021). https://doi.org/10.1007/s00366-019-00931-w

2. S.-X. Chen, S. Sahmani, B. Safaei, Size-dependent nonlinear bending behavior of porous FGM quasi-3D microplates with a central cutout based on nonlocal strain gradient isogeometric finite element modelling. Eng. Comput. **37**, 1657–1678 (2021). https://doi.org/10.1007/s00366-021-01303-z

3. X. Yang, S. Sahmani, B. Safaei, Postbuckling analysis of hydrostatic pressurized FGM microsized shells including strain gradient and stress-driven nonlocal effects. Eng. Comput. **37**, 1549–1564 (2021). https://doi.org/10.1007/s00366-019-00901-2

4. D.X. Hung, T.M. Tu, L.N. Van, P.H. Anh, Nonlinear buckling and postbuckling of FG porous variable thickness toroidal shell segments surrounded by elastic foundation subjected to compressive loads. Aerosp. Sci. Technol. **107**, 106253 (2020). https://doi.org/10.1016/j.ast.2020.106253

5. R. Moradi-Dastjerdi, K. Behdinan. Layer arrangement impact on the electromechanical performance of a five-layer multifunctional smart sandwich plate. In: K. Behdinan, R. Moradi-Dastjerdi, (eds.) *Adv. Multifunct. Light. Aerostructures Des. Dev. Implement*. 1st ed., Hoboken: John Wiley & Sons Ltd; (2021), p. 3–24

6. H. Lin, D. Cao, Y. Xu, Vibration characteristics and flutter analysis of a composite laminated plate with a store. Appl Math Mech English Ed **9**, 241–260 (2018). https://doi.org/10.1007/s10483-018-2297-6

7. M. Alhijazi, Q. Zeeshan, Z. Qin, B. Safaei, M. Asmael, Finite element analysis of natural fibers composites: a review. Nanotechnol. Rev. **9**, 853–875 (2020). https://doi.org/10.1515/ntrev-2020-0069

8. R. Moradi-Dastjerdi, G. Payganeh, Thermoelastic dynamic analysis of wavy carbon nanotube reinforced cylinders under thermal loads. Steel Compos. Struct. **25**, 315–326 (2017). https://doi.org/10.12989/scs.2017.25.3.315

9. A.M. Fattahi, B. Safaei, Z. Qin, F. Chu, Experimental studies on elastic properties of high density polyethylene-multi walled carbon nanotube nanocomposites. Steel Compos. Struct. **38**, 187 (2021). https://doi.org/10.12989/scs.2021.38.2.177

10. S. Karimzadeh, B. Safaei, T.C. Jen, Investigate the importance of mechanical properties of SWCNT on doxorubicin anti-cancer drug adsorption for medical application: A molecular dynamic study. J. Mol. Graph. Model **101**, 107745 (2020). https://doi.org/10.1016/j.jmgm.2020.107745

11. E. Magnucka-Blandzi, K. Wisniewska-Mleczko, M.J. Smyczynski, P. Kedzia, Buckling of a sandwich symmetrical circular plate with varying mechanical properties of the core. Appl. Math. Mech. English Ed **39**, 981–992 (2018). https://doi.org/10.1007/s10483-018-2347-8

12. J.R. Vinson, Sandwich structures. Appl. Mech. Rev. **54**, 201 (2001). https://doi.org/10.1115/1.3097295

13. R. Moradi-Dastjerdi, S.A. Meguid, S. Rashahmadi, Electro-dynamic analysis of smart nanoclay-reinforced plates with integrated piezoelectric layers. Appl. Math. Model **75**, 267–278 (2019). https://doi.org/10.1016/j.apm.2019.05.033

14. M. Shaban, H. Mazaheri, Bending analysis of five-layer curved functionally graded sandwich panel in magnetic field: closed-form solution. Appl. Math. Mech. English Ed **42**, 251–274 (2021). https://doi.org/10.1007/s10483-021-2675-7

15. Y. Feng, H. Qiu, Y. Gao, H. Zheng, J. Tan, Creative design for sandwich structures: a review. Int. J. Adv. Robot Syst. (2020). https://doi.org/10.1177/1729881420921327

16. L. Wu, X. Zhang, J. Ban, Q. Jiang, T. Li, J. Lin, Design and optimization of multi-scale porous sandwich composites with excellent sound absorption and cushioning properties. J. Sandw. Struct. Mater. (2021). https://doi.org/10.1177/1099636221993903

17. T. Liu, S. Hou, X. Nguyen, X. Han, Energy absorption characteristics of sandwich structures with composite sheets and bio coconut core. Compos Part B **114**, 328–338 (2017). https://doi.org/10.1016/j.compositesb.2017.01.035

18. R. Moradi-Dastjerdi, K. Behdinan, Thermo-electro-mechanical behavior of an advanced smart lightweight sandwich plate. Aerosp. Sci. Technol. **106**, 106142 (2020). https://doi.org/10.1016/j.ast.2020.106142

19. M.-C. Trinh, D.-D. Nguyen, S.-E. Kim, T.M. Chien, N.D. Duc, S.K. Eock, Effects of porosity and thermomechanical loading on free vibration and nonlinear dynamic response of functionally graded sandwich shells with double curvature. Aerosp. Sci. Technol. **87**, 119–132 (2019). https://doi.org/10.1016/j.ast.2019.02.010

20. M. Esmaeilzadeh, M. Kadkhodayan, Dynamic analysis of stiffened bi-directional functionally graded plates with porosities under a moving load by dynamic relaxation method with kinetic damping. Aerosp. Sci. Technol. **93**, 105333 (2019). https://doi.org/10.1016/j.ast.2019.105333

21. W. Gao, Z. Qin, F. Chu, Wave propagation in functionally graded porous plates reinforced with graphene platelets. Aerosp. Sci. Technol. **102**, 105860 (2020). https://doi.org/10.1016/j.ast.2020.105860

22. Y. Liu, Z. Qin, F. Chu, Nonlinear forced vibrations of FGM sandwich cylindrical shells with porosities on an elastic substrate. Nonlinear Dyn. (2021). https://doi.org/10.1007/s11071-021-06358-7

23. Y. Liu, Z. Qin, F. Chu, Analytical study of the impact response of shear deformable sandwich cylindrical shell with a functionally graded porous core. Mech. Adv. Mater Struct. (2020). https://doi.org/10.1080/15376494.2020.1818904

24. F. Fan, Y. Xu, S. Sahmani, B. Safaei, Modified couple stress-based geometrically nonlinear oscillations of porous functionally graded microplates using NURBS-based isogeometric approach. Comput. Methods Appl. Mech. Eng. **372**, 113400 (2020). https://doi.org/10.1016/j.cma.2020.113400

25. J.L. Mantari, A.S. Oktem, S.C. Guedes, A new trigonometric shear deformation theory for isotropic, laminated composite and sandwich plates. Int. J. Solids Struct. **49**, 43–53 (2012). https://doi.org/10.1016/j.ijsolstr.2011.09.008

26. P. Malekzadeh, A.R. Fiouz, H. Razi, Three-dimensional dynamic analysis of laminated composite plates subjected to moving load. Compos. Struct. **90**, 105–114 (2009). https://doi.org/10.1016/j.compstruct.2009.02.008

27. A.R. Setoodeh, P. Malekzadeh, K. Nikbin, Low velocity impact analysis of laminated composite plates using a 3D elasticity based layerwise FEM. Mater Des. **30**, 3795–3801 (2009). https://doi.org/10.1016/j.matdes.2009.01.031

28. C.H. Thai, A.J.M. Ferreira, E. Carrera, H. Nguyen-Xuan, Isogeometric analysis of laminated composite and sandwich plates using a layerwise deformation theory. Compos. Struct. **104**, 196–214 (2013). https://doi.org/10.1016/J.COMPSTRUCT.2013.04.002

29. T. Yu, S. Yin, T.Q. Bui, S. Xia, S. Tanaka, S. Hirose, NURBS-based isogeometric analysis of buckling and free vibration problems for laminated composites plates with complicated cutouts using a new simple FSDT theory and level set method. Thin. Walled Struct. **101**, 141–156 (2016). https://doi.org/10.1016/j.tws.2015.12.008

30. F. Tornabene, N. Fantuzzi, M. Bacciocchi, J.N. Reddy, A posteriori stress and strain recovery procedure for the static analysis of laminated shells resting on nonlinear elastic foundation. Compos. Part B Eng. **126**, 162–191 (2017). https://doi.org/10.1016/J.COMPOSITESB.2017.06.012

31. R. Xiaohui, W. Zhen, J. Bin, A refined sinusoidal theory for laminated composite and sandwich plates. Mech. Adv. Mater Struct. (2018). https://doi.org/10.1080/15376494.2018.1538469

32. M. Sehoul, M. Benguediab, A. Bakora, A. Tounsi, Free vibrations of laminated composite plates using a novel four variable refined plate theory. Steel Compos. Struct. **24**, 603–613 (2017). https://doi.org/10.12 989/scs.2017.24.5.603

33. H.K. Bisheh, N. Wu, Wave propagation characteristics in a piezoelectric coupled laminated composite cylindrical shell by considering transverse shear effects and rotary inertia. Compos. Struct. **191**, 123–144 (2018). https://doi.org/10.1016/j.compstruct.2018.02.010

34. Z. Wang, T. Yu, T.Q. Bui, N.A. Trinh, N.T.H. Luong, N.D. Duc et al., Numerical modeling of 3-D inclusions and voids by a novel adaptive XFEM. Adv. Eng. Softw. **102**, 105–122 (2016). https://doi.org/ 10.1016/j.advengsoft.2016.09.007

35. N.V. Nguyen, H.X. Nguyen, S. Lee, H. Nguyen-xuan, Geometrically nonlinear polygonal finite element analysis of functionally graded porous plates. Adv. Eng. Softw. **126**, 110–126 (2018). https://doi.org/10. 1016/j.advengsoft.2018.11.005

36. J. Yang, D. Chen, S. Kitipornchai, Buckling and free vibration analyses of functionally graded graphene reinforced porous nanocomposite plates based on Chebyshev-Ritz method. Compos Struct **193**, 281–294 (2018). https://doi.org/10.1016/J.COMPSTRUCT.2018.03.090

37. Y.H. Dong, Y.H. Li, D. Chen, J. Yang, Vibration characteristics of functionally graded graphene reinforced porous nanocomposite cylindrical shells with spinning motion. Compos. Part B Eng. **145**, 1–13 (2018). https://doi.org/10.1016/j.compositesb.2018.03.009

38. M.R. Barati, A.M. Zenkour, Electro-thermoelastic vibration of plates made of porous functionally graded piezoelectric materials under various boundary conditions. J. Vib. Control. **24**, 1910–1926 (2018). https:// doi.org/10.1177/1077546316672788

39. M. Askari, A.R. Saidi, A.S. Rezaei, An investigation over the effect of piezoelectricity and porosity distribution on natural frequencies of porous smart plates. J. Sandw. Struct. Mater. (2018). https://doi.org/ 10.1177/1099636218791092

40. M. Mohammadi, M. Bamdad, K. Alambeigi, R. Dimitri, F. Tornabene, Electro-elastic response of cylindrical sandwich pressure vessels with porous core and piezoelectric face-sheets. Compos. Struct. **225**, 111119 (2019). https://doi.org/10.1016/J.COMPSTRUCT.2019.111119

41. R. Moradi-Dastjerdi, K. Behdinan, B. Safaei, Z. Qin, Static performance of agglomerated CNT-reinforced porous plates bonded with piezoceramic faces. Int. J. Mech. Sci. **188**, 105966 (2020). https://doi.org/10. 1016/j.ijmecsci.2020.105966

42. R. Moradi-Dastjerdi, K. Behdinan, B. Safaei, Z. Qin, Buckling behavior of porous CNT-reinforced plates integrated between active piezoelectric layers. Eng. Struct. **222**, 111141 (2020). https://doi.org/10.1016/ j.engstruct.2020.111141

43. R. Moradi-Dastjerdi, K. Behdinan, Free vibration response of smart sandwich plates with porous CNT-reinforced and piezoelectric layers. Appl. Math. Model (2021). https://doi.org/10.1016/j.apm.2021.03.0 13

44. N.V. Nguyen, J. Lee, H. Nguyen-Xuan, Active vibration control of GPLs-reinforced FG metal foam plates with piezoelectric sensor and actuator layers. Compos. Part B Eng. **172**, 769–784 (2019). https://doi.org/ 10.1016/J.COMPOSITESB.2019.05.060

45. J. Zhao, F. Xie, A. Wang, C. Shuai, J. Tang, Q. Wang, Vibration behavior of the functionally graded porous (FGP) doubly-curved panels and shells of revolution by using a semi-analytical method. Compos. Part B **157**, 219–238 (2019). https://doi.org/10.1016/j.compositesb.2018.08.087

46. O. Zargar, M. Mollaghaee-Roozbahani, M. Bashirpour, M. Baghani, The application of homotopy analysis method to determine the thermal response of convective-radiative porous fins with temperature-dependent properties. Int. J. Appl. Mech. (2019). https://doi.org/10.1142/S1758825119500893

47. M. Babaei, M. Hadi, K. Asemi, Natural frequency and dynamic analyses of functionally graded saturated porous annular sector plate and cylindrical panel based on 3D elasticity. Aerosp. Sci. Technol. **96**, 105524 (2020). https://doi.org/10.1016/j.ast.2019.105524

48. B. Sobhani Aragh, M.H. Yas, Effect of continuously grading fiber orientation face sheets on vibration of sandwich panels with FGM core. Int. J. Mech. Sci. **53**, 628–638 (2011). https://doi.org/10.1016/J. IJMECSCI.2011.05.009

49. R. Moradi-Dastjerdi, K. Behdinan, Temperature effect on free vibration response of a smart multifunctional sandwich plate. J. Sandw. Struct. Mater. (2020). https://doi.org/10.1177/1099636220908707

50. R. Moradi-Dastjerdi, A. Radhi, K. Behdinan, Damped dynamic behavior of an advanced piezoelectric sandwich plate. Compos. Struct. **243**, 112243 (2020). https://doi.org/10.1016/j.compstruct.2020.112243

51. A.R. Setoodeh, M. Shojaee, P. Malekzadeh, Vibrational behavior of doubly curved smart sandwich shells with FG-CNTRC face sheets and FG porous core. Compos. Part B Eng. **165**, 798–822 (2019). https:// doi.org/10.1016/J.COMPOSITESB.2019.01.022

52. B. Safaei, R. Moradi-Dastjerdi, Z. Qin, K. Behdinan, F. Chu, Determination of thermoelastic stress wave propagation in nanocomposite sandwich plates reinforced by clusters of carbon nanotubes. J. Sandw. Struct. Mater. (2019). https://doi.org/10.1177/1099636219848282

53. A. Amiri, M. Mohammadimehr, M. Anvari, Stress and buckling analysis of a thick-walled micro sandwich panel with a flexible foam core and carbon nanotube reinforced composite (CNTRC) face sheets. Appl. Math. Mech. English Ed. **41**, 1027–1038 (2020). https://doi.org/10.1007/s10483-020-2627-7

54. Q. Li, D. Wu, X. Chen, L. Liu, Y. Yu, W. Gao, Nonlinear vibration and dynamic buckling analyses of sandwich functionally graded porous plate with graphene platelet reinforcement resting on Winkler-Pasternak elastic foundation. Int. J. Mech. Sci. **148**, 596–610 (2018). https://doi.org/10.1016/J.IJMECSCI.2018.09.020

55. R. Moradi-Dastjerdi, K. Behdinan, Stress waves in thick porous graphene-reinforced cylinders under thermal gradient environments. Aerosp. Sci. Technol. **110**, 106476 (2021). https://doi.org/10.1016/j.ast.2020.106476

56. B. Safaei, The effect of embedding a porous core on the free vibration behavior of laminated composite plates. Steel Compos. Struct. **35**, 659–670 (2020). https://doi.org/10.12989/SCS.2020.35.5.659

57. Reddy JN. Mechanics of Laminated Composite Plates and Shells: Theory and Analysis. CRC press; 2004.

58. M. Mohammadsalehi, O. Zargar, M. Baghani, Study of non-uniform viscoelastic nanoplates vibration based on nonlocal first-order shear deformation theory. Meccanica **52**, 1063–1077 (2017). https://doi.org/10.1007/s11012-016-0432-0

59. R. Talebitooti, K. Daneshjoo, S.A.M. Jafari, Optimal control of laminated plate integrated with piezo-electric sensor and actuator considering TSDT and meshfree method. Eur. J. Mech. A/Solids **55**, 199–211 (2016). https://doi.org/10.1016/j.euromechsol.2015.09.004

60. A.H. Baferani, A.R. Saidi, H. Ehteshami, Accurate solution for free vibration analysis of functionally graded thick rectangular plates resting on elastic foundation. Compos. Struct. **93**, 1842–1853 (2011)

61. H. Thai, D. Choi, A refined plate theory for functionally graded plates resting on elastic foundation. Compos. Sci. Technol. **71**, 1850–1858 (2011). https://doi.org/10.1016/j.compscitech.2011.08.016